ACS APPLIED MATERIALS & INTERFACES

Research Article

www.acsami.org

Computational Analysis of Stable Hard Structures in the Ti−B System

Pengfei Li,[†,§] Rulong Zhou,*[,‡] and Xiao Cheng Zeng*[,§,†]

[†]Hefei National Laboratory for Physical Sciences at Microscale and Department of Chemical Physics, University of Science and Technology of China, Hefei, Anhui 230026, China

[‡]School of Science and Engineering of Materials, Hefei University of Technology, Hefei, Anhui 230009, China

[§]Department of Chemistry and Department of Mechanical and Materials Engineering, University of Nebraska—Lincoln, Lincoln, Nebraska 68588, United States

Supporting Information

ABSTRACT: The lowest energy crystalline structures of various stoichiometric titanium boride (Ti−B) intermetallic compounds are sought based on density functional theory combined with the particle-swarm optimization (PSO) technique. Besides three established experimental structures, i.e., FeB-type TiB, AlB_2-type, and Ta_3B_4-type Ti_3B_4, we predict additional six metastable phases at these stoichiometric ratios, namely, α- and β-phases for TiB, TiB_2, and Ti_3B_4, respectively. Moreover, we predict the most stable crystalline structures of four new titanium boride compounds with different stoichiometric ratios: Ti_2B−PS_A, Ti_2B_3−PS_B, TiB_3−PS_C, and TiB_4−PS_D. Notably, Ti_2B−PS_A is shown to have lower formation energy (thus higher stability) than the previously proposed Al_2Cu-type Ti_2B. The computed convex-hull and phonon dispersion relations confirm that all the newly predicted Ti−B intermetallic crystals are thermodynamically and dynamically stable. Remarkably, the predicted α-TiB_2 and β-TiB_2 show semi-metal-like electronic properties and possess high Vickers hardnesses (39.4 and 39.6 GPa), very close to the lower limit of *superhard materials* (40 GPa). Analyses of band structure, density of states, electronic localization function, and various elastic moduli provide further understanding of the electronic and mechanical properties of the intermetallic titanium borides. We hope the newly predicted hard intermetallic titanium borides coupled with desirable electronic properties and high elastic modulus will motivate future experimental synthesis for applications such as high-temperature structural materials.

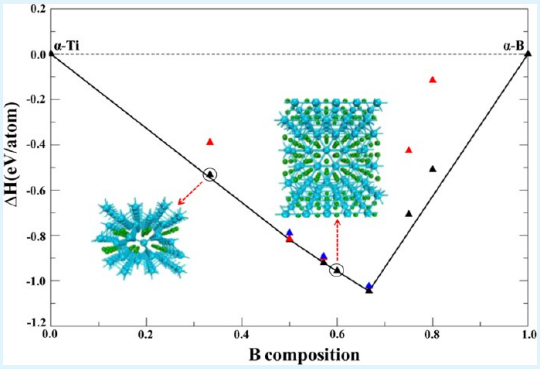

KEYWORDS: *titanium boride compounds, particle-swarm optimization technique, density functional theory, electronic structures, mechanical properties, hard electronic materials*

INTRODUCTION

Transition-metal borides belong to a class of intermetallic compounds, and they are of both fundamental and practical importance owing to their excellent mechanical, thermal, and chemical properties. Several transition-metal borides exhibit *near-superhard* properties which endow them as promising applications in various sectors of industry, such as in wear-resistant coatings of mechanical components or as cutting, grinding, and polishing tools.[1−6] Recently, great efforts have been devoted to study this new type of near-superhard materials. Previous experimental studies reveal that ReB_2[7,8]and and WB_4[9] are both near-superhard materials with measured hardnesses up to 36.4−48 and 46.2 GPa, respectively. A recent theoretical study of the mechanical properties of Mn−B systems[10] shows that MnB_4 and ReB_2-type MnB_2 also exhibit relatively high hardness. As a same row transition metal element in the periodic table as Mn, titanium (Ti) also possesses a low compressibility. Hence, it is timely to explore possible superhard titanium boride materials for future applications as high-temperature structural materials (e.g., as a cathode material).

Today, crystalline structures of three Ti−B intermetallic compounds are already known from experimental measurements, i.e., TiB, TiB_2, and Ti_3B_4. Decker and Kasper[11] were the first to report that TiB crystallizes into the FeB-type structure, a primitive orthorhombic (*Pnma*) crystal belonging to the *mmm* point group. TiB_2 belongs to the hexagonal crystalline system with the space group *P6/mmm*.[12] Ti_3B_4 has an orthorhombic Ta_3B_4-type structure with the space group *Immm*, revealed by Spear et al.[13] Among the three titanium borides, the AlB_2-type TiB_2 is the most well-known and has attracted considerable experimental and theoretical attention.[14−19] Nevertheless, TiB whiskers, as reinforcement, can be used in various titanium alloys,[20] while Ti_3B_4 is a potential high-temperature-resistant material.[21] Besides the aforementioned three Ti−B intermetal-

Received: May 19, 2015
Accepted: June 30, 2015
Published: June 30, 2015

DOI: 10.1021/acsami.5b04332
ACS Appl. Mater. Interfaces 2015, 7, 15607−15617

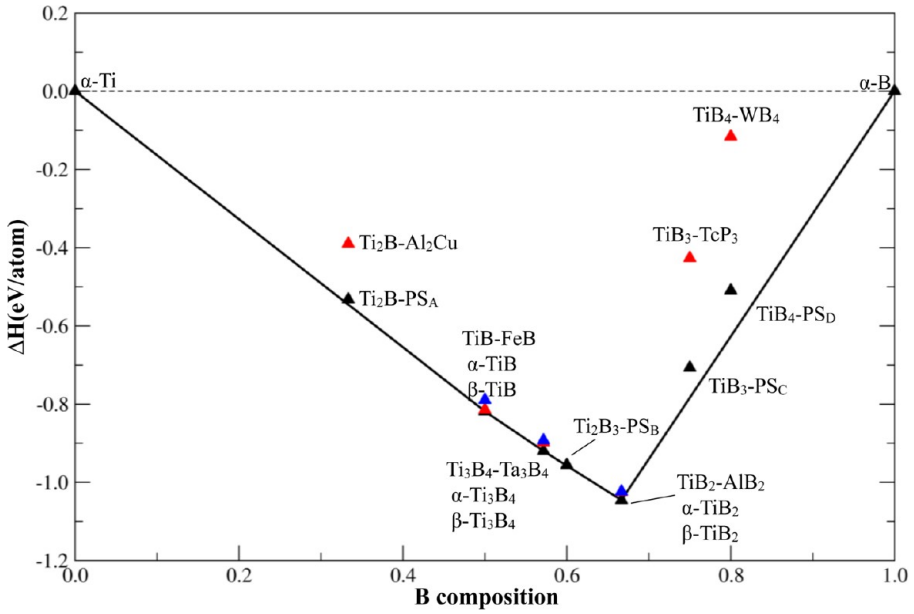

Figure 1. Computed formation enthalpy vs composition curves for stoichiometric titanium boride compounds. The solid line denotes the ground-state convex hull.

lic compounds, few studies have been reported on crystalline structures of other titanium borides with different stoichiometry. It would be desirable to uncover new Ti−B crystals with novel physical properties. Here, we report an extensive search of the most stable structures of titanium borides with seven stoichiometric ratios of Ti/B and a systematic study of their structural and physical properties, including dynamic stability, structural, mechanical, and electronic properties. The seven Ti−B compounds with different stoichiometric ratios considered include the known TiB, TiB_2, and Ti_3B_4, as well as new Ti_2B, Ti_2B_3, TiB_3, and TiB_4.

COMPUTATIONAL METHODS

The search for the lowest energy crystalline structures of various stoichiometric titanium borides is based on the particle-swarm optimization (PSO) algorithm implemented in the CALYPSO package.[22] The PSO algorithm belongs to the evolutionary algorithm. The latter has been benchmark tested for many known systems with various chemical bonding and is able to predict the most stable and low-energy metastable two-dimensional (2D) and 3D solid-state structures of various elements and compounds at different pressures.[23−28] Specifically, in our CALYPSO crystal search, the population size of each generation is set to be 40−60 (the population size increases with the size of the simulation cell), and the maximum number of generations is typically 30. The population of Ti−B crystalline structures in the first generation is generated randomly with the constraint of symmetry. In the ensuing generations, 60% of the population is generated from the best (lowest energy) structures in the previous generation by using the PSO scheme and the other 40% is generated randomly to ensure diversity of the population. Local optimization including the atomic positions and lattice parameters is then performed for all of the initial structures. To search the most stable structure for each of the seven stoichiometric ratios, different simulation cells containing two, four, six, or eight Ti_mB_n units are taken into account. For Ti_3B_4, a simulation cell containing up to four units is considered.

The structure relaxation and total-energy calculation are performed using the density functional theory within the generalized gradient approximation (GGA),[29] as implemented in the VASP 5.3 package.[30] All-electron plane-wave basis sets with the projector augmented wave (PAW) potentials are adopted with $2s^22p^1$and $3d^24s^2$ treated as valence electron configuration for B and Ti, respectively. The cutoff energy for expansion of the wave function into plane waves is set to be 445 eV, and a dense *k*-point sampling with the grid spacing less than $2\pi \times 0.02$ Å^{-1} in the Brillouin zone is used. The computed total energy is converged within 1 meV/atom. For geometric optimization, both lattice constants and atomic positions are relaxed until the forces on atoms are less than 0.01 eV/ Å and the total-energy change is less than 1×10^{-5} eV. Phonon spectra of the predicted crystalline structures are computed using the VASP package coupled with the PHONOPY program.[31] The phonon−spectrum calculation is to confirm dynamic stability of the obtained crystal structures. Note that all total energies are computed for the solid systems at temperature of 0 K and ambient pressure.

RESULTS AND DISCUSSION

Through the PSO search, a larger number of low-energy crystalline structures of titanium borides are obtained. The predicted lowest energy structures of TiB, TiB_2, and Ti_3B_4 are indeed the same as experimental structures, not only lending credence to the PSO search method but also indicating that the predictions are consistent with accepted phase equilibria in the Ti−B system. The three crystalline structures are denoted as TiB−FeB (*Pnma*, No. 62), TiB_2−AlB_2(*P6/mmm*, No. 191), and Ti_3B_4−Ta_3B_4 (*Immm*, No. 71) for TiB, TiB_2 and Ti_3B_4 compounds, respectively. Besides the lowest energy structures, several promising metastable structures whose energies are within 30 meV/atom of the value of the lowest energy structures are also obtained for the three stoichiometric ratios. We denote these metastable structures as α-TiB, β-TiB; α-TiB_2, β-TiB_2; and α-Ti_3B_4, β-Ti_3B_4, representing the second and third lowest energy structures of TiB, TiB_2, and Ti_3B_4, respectively. For the new stoichiometric ratios considered (i.e., Ti_2B, Ti_2B_3, TiB_3, and TiB_4), the predicted lowest energy crystals are denoted as Ti_2B−PS_A (*Pmn*2_1, No. 31, hereafter denoted as PS_A), Ti_2B_3−PS_B (*Cmcm*, No. 63), TiB_3−PS_C (*C2/m*, No. 12), and TiB_4−PS_D (*Amm*2, No. 38), respectively. In addition, a crystalline structure reported in the literature, namely, Ti_2B−Al_2Cu (*I*4/*mcm*, No. 140)[32] is also examined. We have also created three crystalline structures by hand using known crystalline structures for other compounds,[9,33,34] i.e, TcP_3, WB_4,

DOI: 10.1021/acsami.5b04332
ACS Appl. Mater. Interfaces 2015, 7, 15607−15617

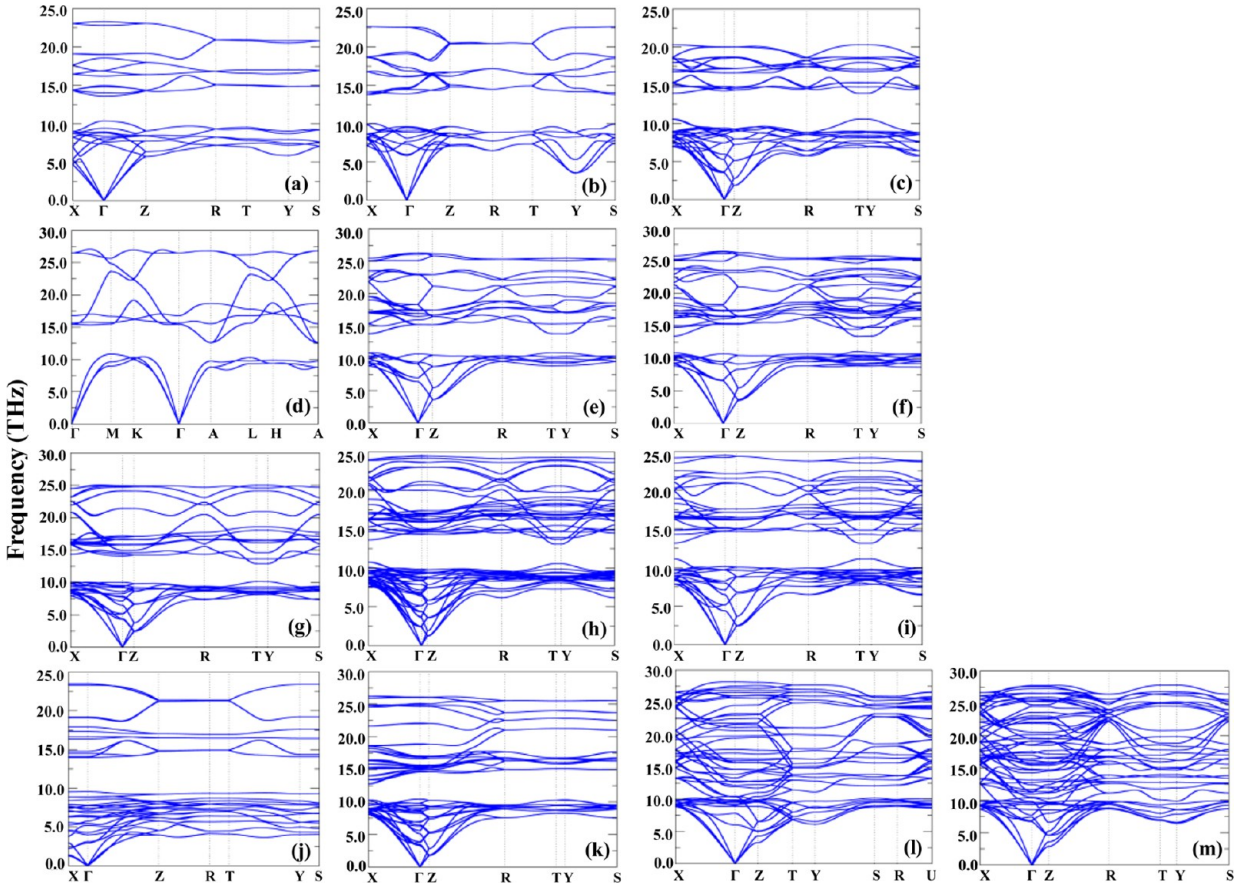

Figure 2. Computed phonon spectra of the Ti−B crystalline structures: (a) TiB−FeB, (b) α-TiB, (c) β-TiB, (d) Ti_2−AlB_2, (e) α-TiB_2, (f) β-TiB_2, (g) Ti_3B_4−Ta_3B_4, (h) α-Ti_3B_4, (i) β-Ti_3B_4, (j) Ti_2B−PS_A, (k) Ti_2B_3−PS_B, (l) TiB_3−PS_C, and (m) TiB_4−PS_D.

and YB_4. Hence the three new crystalline structures are named as TiB_3−TcP_3 (*Pnma*, No. 62), TiB_4−WB_4 ($P6_3/mmc$, No. 194), and TiB_4−YB_4 ($P4/mbm$, No. 127) for the purpose of comparison.

A. Formation Enthalpy and Phase Stability. Formation enthalpies can be used to assess relative stability of crystalline compounds at low temperatures and to construct a quantitative convex-hull plot. The formation enthalpy for titanium boride compounds can be defined as follows:

$$\Delta H = [H(\mathrm{Ti}_m\mathrm{B}_n) - mH(\mathrm{Ti}_{\mathrm{bulk}}) - nH(\mathrm{B}_{\mathrm{bulk}})]/(m + n) \quad (1)$$

where H is the enthalpy of either a compound or a constituent element at a specific pressure. Here, α-B and α-Ti phases are used as the reference structures for solid boron and titanium, respectively, because the two structures are the most stable at the simulation temperature and pressure.

To validate stability of these Ti−B crystalline phases, the convex hull of the formation enthalpy is plotted (see Figure 1), where the structure whose formation enthalpy is located at the local minimum of the convex hull is stable against decomposition into phases of the neighboring compositions and can be fabricated in principle.[35,36] As shown in Figure 1, four compounds are located at the local minima of the convex hull, which are TiB−FeB, Ti_3B_4−Ta_3B_4, Ti_2B_3−PS_B, and TiB_2−AlB_2. Among them, TiB−FeB, Ti_3B_4−Ta_3B_4, and TiB_2−AlB_2 are already observed experimentally while Ti_2B_3−PS_B is a new ground-state structure predicted. These results show that our crystalline structure search strategy is sufficient to locate the ground-state structures of Ti−B compounds. Besides these lowest enthalpy structures, we also find some low-enthalpy metastable structures which may be fabricated in the laboratory as well. As shown in Figure 1, the formation enthalpy of Ti_2B−PS_A is much lower than that of a previously proposed structure Ti_2B−Al_2Cu, [32] and it lies slightly above the curve of convex hull (about 10 meV/atom), suggesting the possibility that the compound could be formed under specific temperature and pressure conditions that would promote its stability. For TiB, Ti_3B_4, and TiB_2, besides the lowest enthalpy structures, two metastable structures (denoted as α and β phases, respectively) for each stoichiometry are found from our structure search; both are very close to the ground state in the formation enthalpy (within 30 meV/atom). Hence, these metastable structures may be also synthesized experimentally under specific temperature and pressure conditions. For TiB_3 and TiB_4, although the lowest enthalpy structures TiB_3−PS_C and TiB_4−PS_D are located above the convex-hull line by 65−100 meV/atom, both structures are more stable than the three crystalline structures, namely, TiB_3−TcP_3, TiB_4−WB_4, and TiB_4−YB_4, where the notations after the dash refer to the TcP_3, WB_4, and YB_4 structures proposed in previous literature.[9,33,34] We expect that both lowest enthalpy structures can be synthesized in specific conditions (e.g., at high temperatures or high pressures).

Furthermore, to confirm that the predicted Ti−B crystalline structures are dynamically stable, phonon spectra of all the predicted structures are computed using the supercell frozen phonon theory implemented in PHONOPY program[31] (see

DOI: 10.1021/acsami.5b04332
ACS Appl. Mater. Interfaces 2015, 7, 15607−15617

Table 1. Calculated Formation Enthalpy per Atom, ΔH (eV/atom), Space Group, Optimized Lattice Parameters *a*, *b*, and *c* (Å), and Cell Volume (V, Å^3) of the Primitive Cell of Titanium Boride Compounds

	structure	space group	ΔH	*a*		*b*		*c*		*V*
TiB	TiB–FeB	*Pnma* (No. 62)	−0.818	6.113	6.121[a]	3.050	3.061[a]	4.562	4.561[a]	85.056
	α-TiB	*Cmcm* (No. 63)	−0.814	3.283		8.480		3.051		84.939
	β-TiB	$I4_1/amd$ (No. 141)	−0.789	3.151		3.151		17.069		169.743
TiB_2	TiB_2–AlB_2	*P6/mmm* (No. 191)	−1.045	3.034	3.028[b]	3.034	3.028[b]	3.225	3.230[b]	25.712
	α-TiB_2	$I4_1/amd$ (No. 141)	−1.024	3.114		3.114		10.551		102.296
	β-TiB_2	$P4_2/mmc$ (No. 131)	−1.023	3.114		3.114		10.550		102.325
Ti_3B_4	Ti_3B_4–Ta_3B_4	*Immm*(No. 71)	−0.920	3.260	3.259[b]	13.742	13.730[b]	3.039	3.032[b]	136.166
	α-Ti_3B_4	*Imm2* (No. 44)	−0.898	3.082		3.193		27.598		271.550
	β-Ti_3B_4	$P4_2/mmc$ (No. 131)	−0.893	3.133		3.133		13.821		135.675
Ti_2B	Ti_2B–PS_A	$Pmn2_1$(No. 31)	−0.533	11.169		4.565		3.028		154.402
	Ti_2B–Al_2Cu	$I4/mcm$ (No. 140)	−0.390							
Ti_2B_3	Ti_2B_3–PS_B	*Cmcm* (No. 63)	−0.956	3.243		3.038		19.025		187.433
TiB_3	TiB_3–PS_C	*C2/m* (No. 12)	−0.707	3.059		5.249		8.128		130.252
	TiB_3–TcP_3	*Pnma* (No. 62)	−0.427							
TiB_4	TiB_4–PS_D	*Amm2* (No. 38)	−0.510	3.089		5.251		9.630		156.198
	TiB_4–WB_4	$P6_3/mmc$ (No. 194)	−0.117							
	TiB_4–YB_4	*P4/mbm* (No. 127)	−0.120							

[a]Reference 11. [b]Reference 13.

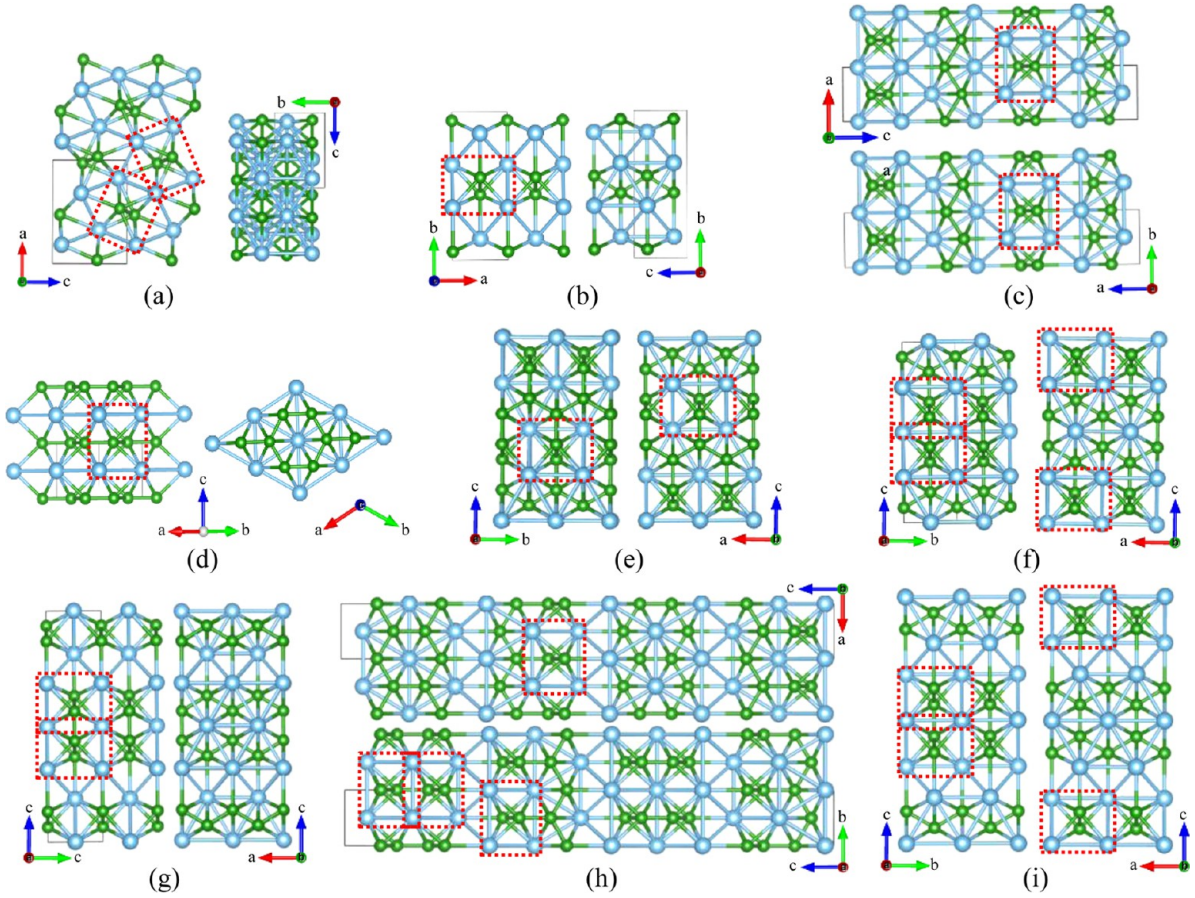

Figure 3. Two views of the atomic structures: (a) TiB-FeB, (b) α-TiB, (c) β-TiB, (d) TiB_2–AlB_2, (e) α-TiB_2, (f) β-TiB_2, (g) Ti_3B_4–Ta_3B_4, (h) α-Ti_3B_4, and (i) β-Ti_3B_4. The green spheres represent B atoms, and silver spheres represent Ti atoms.

Figure 2). According to phonon theory,[37] a solid structure with negative phonon frequencies would be unstable and tend to transform to a lower energy structure. However, if a system is located at its local minima on the potential energy surface, no negative frequencies will appear. Clearly, no negative phonon frequencies are seen over the entire Brillouin zones for all the predicted Ti–B crystalline structures, indicating likely inherent dynamical stability for these titanium borides.

B. Detailed Crystalline Structural Features. Optimized structure parameters and formation enthalpies of titanium boride compounds with different stoichiometric ratios are listed in Table 1. The formation enthalpies are negative for all Ti–B

DOI: 10.1021/acsami.5b04332
ACS Appl. Mater. Interfaces 2015, 7, 15607–15617

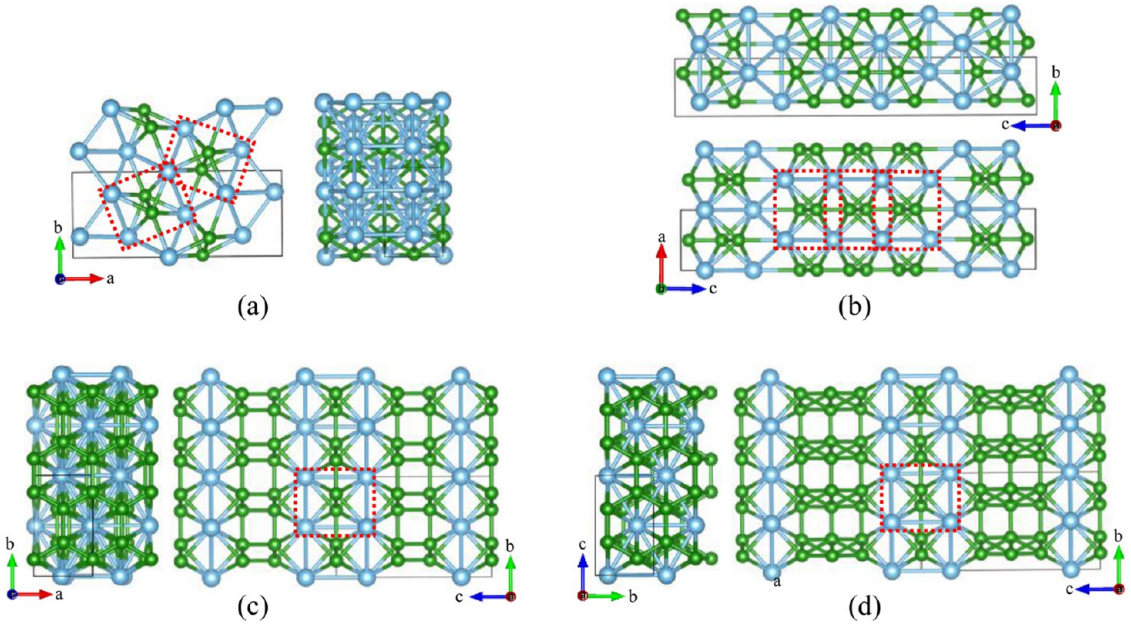

Figure 4. Two views of the atomic structure: (a) Ti_2B-PS_A, (b) Ti_2B_3−PS_B, (c) TiB_3−PS_C, and (d) TiB_4−PS_D. The green spheres represent B atoms, and silver spheres represent Ti atoms.

crystalline structures predicted, indicating that they are all thermodynamically stable at low temperature with respect to the constituent elements (Ti and B). Among these titanium boride compounds, TiB_2−AlB_2 possesses the lowest formation enthalpy. The calculated lattice parameters for the three known titanium boride compounds are in very good agreement with the experimental values.

For TiB−FeB, α-TiB, and β-TiB, the unit cell has four Ti and four B atoms (see red rectangles in Figure 3a−c). In their crystalline structures, each B atom is bonded with six Ti atoms, forming a trigonal prism (Ti_6B) which is the fundamental building block of all three crystals. By stacking the Ti_6B building blocks in the way of sharing a side face of the trigonal prism, the trigonal-prism chain is constructed. Next, the trigonal-prism chains with different orientations are connected with one another, giving one of the three structures of TiB. As shown in Figure 3a, in TiB−FeB, there are two different types of trigonal-prism chains, both aligned along the [010] direction. The difference between the two types of trigonal-prism chains is due to different orientation of the Ti_6B building blocks. The angle between the orientations of the Ti_6B building blocks in the two chains is about 150°. In α-TiB, there is only one type of trigonal-prism chain. The trigonal-prism chains form a slab through connecting with one another in the way of sharing the top face of the trigonal prism (Figure 3b). The slabs then stack along the [010] direction, giving the crystalline structure of α-TiB. The structure of β-TiB is somewhat similar to that of α-TiB, which can be also viewed as stacking slabs formed by trigonal-prism chains. The structure difference between α-TiB and β-TiB is that the slabs in α-TiB are all in the same orientation (defined as the direction of the trigonal-prism chains) while those in β-TiB are perpendicular to their neighboring slabs.

The most stable crystalline phase of TiB_2 is the well-known AlB_2-type with Ti and B atoms located at the origin and (1/3, 2/3, 1/2) sites, while the coplanar graphite-like B layers are present alternatively with the close-packed Ti sheets (see Figure 3d). It can be also viewed as stacking Ti_6B trigonal prisms with shared top and side faces between adjacent ones. The two metastable TiB_2 phases, α-TiB_2 and β-TiB_2, belong to a tetragonal crystalline system, and there are 8B atoms and 4Ti atoms in the unit cell (Figure 3e,f). The structure of α-TiB_2 is somewhat similar to that of α-TiB. In α-TiB_2, the slabs constructed by trigonal-prism chains are stacked with one another with the insertion of one B layer between them, while in α-TiB they are stacked directly with one another. α-TiB_2 can be also viewed as an alternative stacking of two perpendicularly oriented trigonal-prism slabs via sharing the corner Ti atoms. Similarly, for β-TiB_2, the structure can be viewed as an alternative stacking of two perpendicularly oriented double-layer trigonal-prism slabs via sharing the corner Ti atoms.

For Ti_3B_4, the most stable crystal exhibits Ta_3B_4-type structure whose orthorhombic unit cell contains 8B and 6Ti atoms (Figure 3g). The metastable crystal β-Ti_3B_4 has the tetragonal unit cell which contains 8B and 6Ti atoms (Figure 3i), while the α-Ti_3B_4 crystal has a relatively large unit cell that contains 16B and 12Ti atoms (Figure 3h). Structurally, Ti_3B_4−Ta_3B_4 can be constructed by stacking double-layered trigonal-prism slabs, while β-Ti_3B_4 can be constructed by the alternative stacking of two perpendicularly oriented double-layer trigonal-prism slabs, which is similar to β-TiB_2 but without sharing the corner Ti atoms between the two differently oriented double-layer slabs. α-Ti_3B_4 can be also constructed by alternatively stacking two different kinds of double-layer trigonal-prism slabs. One is the same as that in Ti_3B_4−Ta_3B_4, while the other can be constructed by stacking two perpendicularly oriented single-thickness trigonal-prism slabs.

Different from the previously proposed structure[32] (tetragonal lattice), Ti_2B−PS_A, the predicted lowest enthalpy structure of Ti_2B possesses an orthorhombic structure with 4B and 8Ti atoms in the unit cell (Figure 4a). It can be viewed as stacking Ti_6B trigonal-prism slabs with the Ti layers inserted between neighboring slabs. Each Ti_6B trigonal-prism slab is composed of two differently oriented Ti_6B chains. The angle between the two chains is about 150°, similar to that in the structure of TiB−FeB. The predicted Ti_2B_3−PS_B is also an orthorhombic

DOI: 10.1021/acsami.5b04332
ACS Appl. Mater. Interfaces 2015, 7, 15607−15617

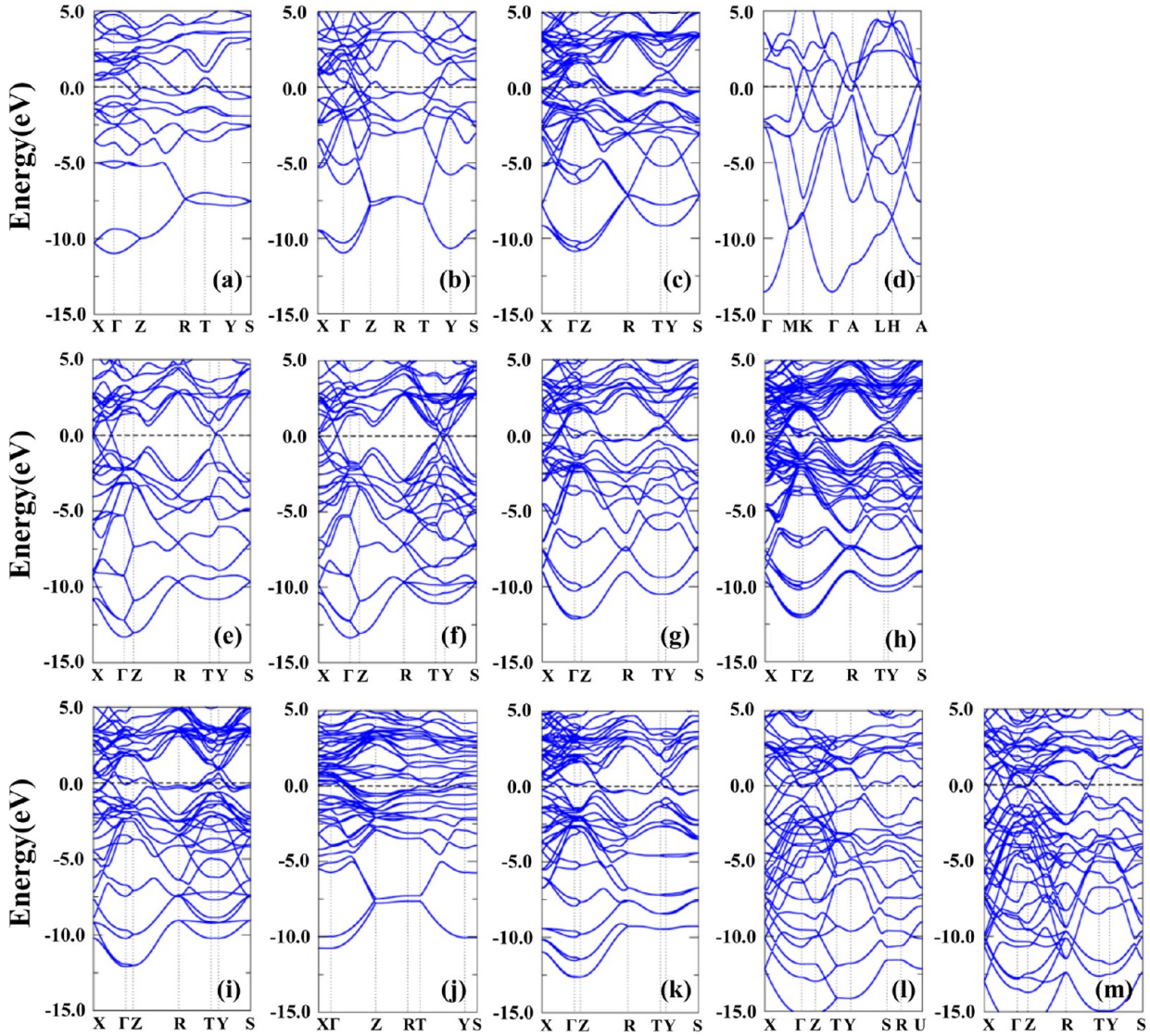

Figure 5. Computed electronic band structures of (a) TiB–FeB, (b) α-TiB, (c) β-TiB, (d) TiB_2–AlB_2, (e) α-TiB_2, (f) β-TiB_2, (g) Ti_3B_4–Ta_3B_4, (h) α-Ti_3B_4, (i) β-Ti_3B_4, (j) Ti_2B–PS_A, (k) Ti_2B_3–PS_B, (l) TiB_3–PS_C, and (m) TiB_4–PS_D. The Fermi level (horizontal dashed line) is set to 0 eV.

crystal with the unit cell containing 12B and 8Ti atoms (Figure 4b). It can be constructed by stacking three-layer Ti_6B trigonal-prism slabs. TiB_3–PS_C exhibits a low-symmetry monoclinic lattice with 12B and 4Ti atoms in the unit cell, while TiB_4–PS_D exhibits an orthorhombic unit cell containing 16B and 4Ti atoms (see Figure 4c,d). Both crystalline structures can be viewed as stacking single-layer Ti_6B trigonal-prism slabs with multilayer B slabs due to higher abundance of B. The structural difference between TiB_3–PS_C and TiB_4–PS_D is that each B slab contains two B layers in TiB_3–PS_C but three B layers in TiB_4–PS_D. Overall, all the stable crystalline structures considered here can be viewed as stacking Ti_6B trigonal-prism slabs with or without the insertion of Ti or B layers. Hence, Ti_6B trigonal prism is the structural motif of the stable crystalline structures of Ti–B compounds.

Electronic Properties and Chemical Bonding. Electronic band structures of the Ti–B compounds considered are computed based on GGA-PBE functional (see Figure 5). Clearly, all of the Ti–B crystals exhibit electrical properties of metals because the Fermi level crosses the energy bands for each system. Among the Ti–B crystals, the α-TiB_2 and β-TiB_2 exhibit very interesting band structures (see Figure 5e,f); that is, two bands cross at the Fermi level, akin to the Dirac points in the band structures of graphene, indicating semi-metal-like electronic properties. Thus, the band gap of α-TiB_2 and β-TiB_2 could be opened via a certain strategy such as strain-tuning or doping.

In Figures 6 and 7, the computed total and partial density of states (TDOS and PDOS) are plotted. It can be seen that the s states of B have little contribution to the TDOS over the energy window of −6.0 to 4.0 eV. The TDOS near the Fermi level is largely contributed to by the Ti 3d states, so the metallic properties of the titanium borides are mainly due to the Ti 3d electrons. It is worth noting that, for all the compounds, the PDOS of Ti 3d and B 2p have similar shape from about −4 to −1.5 eV, indicating that there is significant hybridization between the Ti 3d and B 2p orbitals. As a result, strong Ti–B covalent bonds are present in these compounds. Notably, the DOS of α-TiB_2 and β-TiB_2 at the Fermi level is close to zero, indicating again that Dirac-like points are present for both crystals. As such, α-TiB_2 and β-TiB_2 may have potential

DOI: 10.1021/acsami.5b04332
ACS Appl. Mater. Interfaces 2015, 7, 15607−15617

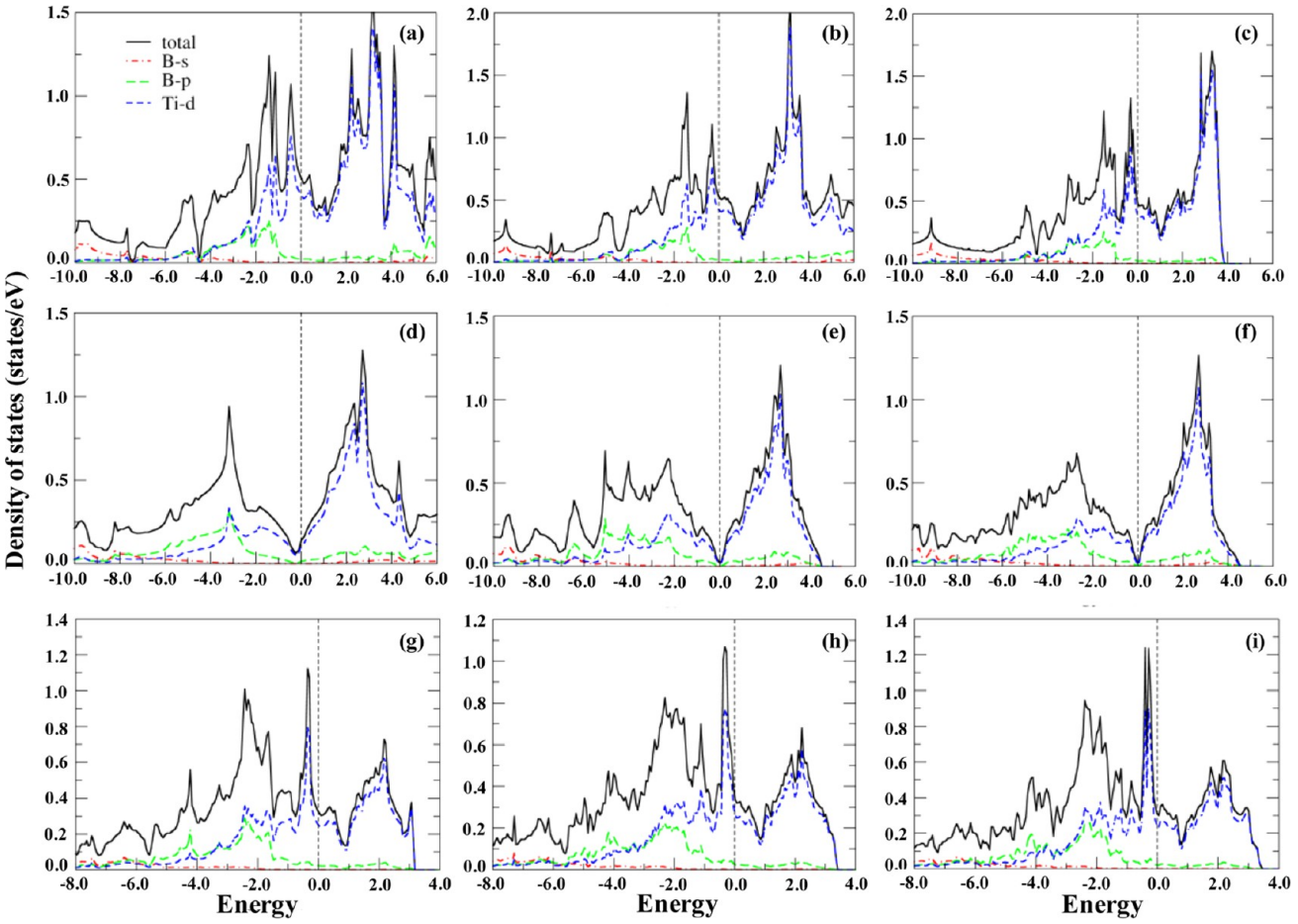

Figure 6. Computed total and partial density of states (DOS) of (a) TiB−FeB, (b) α-TiB, (c) β-TiB, (d) TiB_2−AlB_2, (e) α-TiB_2, (f) β-TiB_2, (g) Ti_3B_4−Ta_3B_4, (h) α-Ti_3B_4, and (i) β-Ti_3B_4. The Fermi level is set to 0 eV.

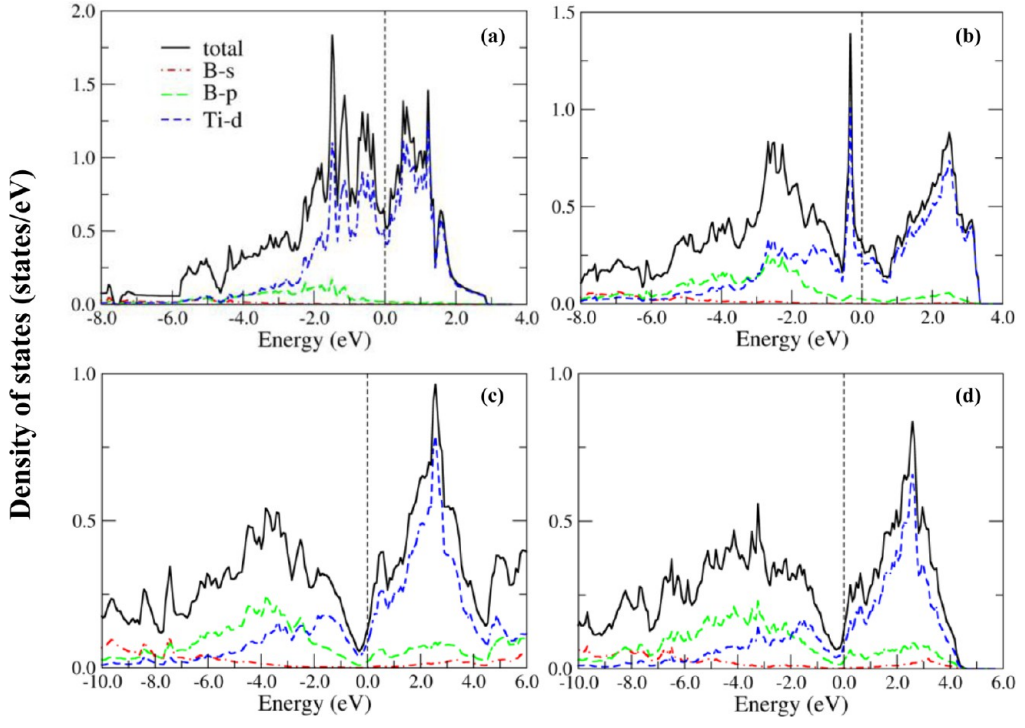

Figure 7. Computed total and partial density of states of (a) Ti_2B−PS_A, (b) Ti_2B_3−PS_B, (c) TiB_3−PS_C, and (d) TiB_4−PS_D.The Fermi level is set to 0 eV.

DOI: 10.1021/acsami.5b04332
ACS Appl. Mater. Interfaces 2015, 7, 15607−15617

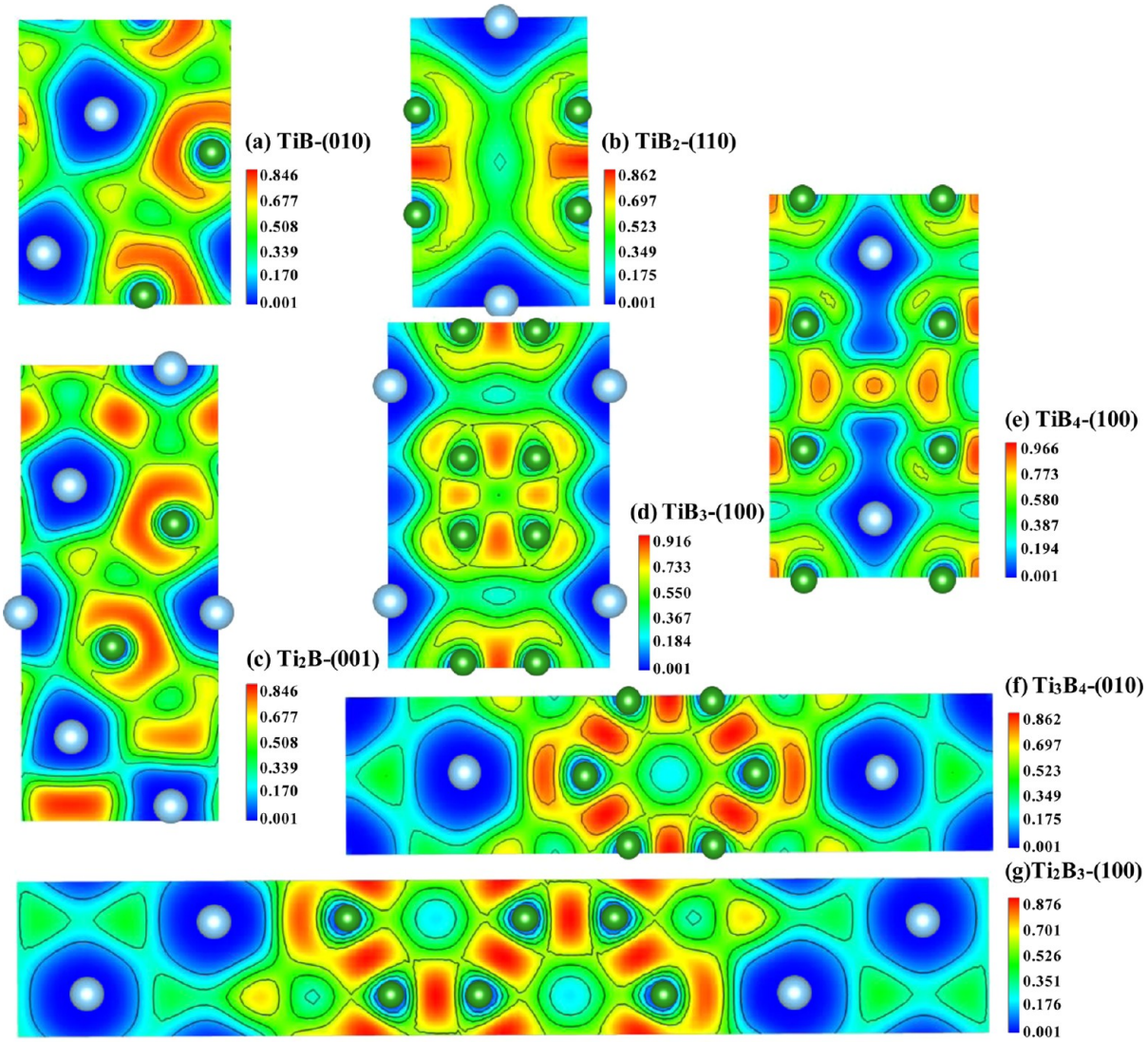

Figure 8. (a–g) Computed 2D ELF for all the Ti–B compounds considered. Note that all B and Ti atoms are exactly in the relevant crystal plane except for the case of 2D ELF for TiB_3-(100), in which four B atoms at the central zone are about 0.4 Å away from the (100) plane.

applications as high-temperature electronic materials, e.g., electrodes in metal smelting.

Moreover, in Figures 6 and 7, a common feature in the TDOS can be seen for most compounds, that is, the presence of a so-called "pseudogap" (a sharp valley around the Fermi level), which represents a borderline between the bonding and antibonding orbitals.[38] The presence of the pseudogap enhances the stability of the compounds. Two possible mechanisms that can offer an explanation to the formation of pseudogap in the binary alloys are the iconicity and the hybridization. However, the electronegativity difference between Ti and B is small (about 0.5); hence the iconicity should play little role in the bonding behavior of these compounds. The pseudogap is most likely due to covalent hybridization between Ti and B atoms.

To gain deeper insights into the bonding nature in the Ti–B compounds, we compute the electron localization function (ELF) which can describe the bond type between atoms: ELF = 1 corresponds to the electrons of perfect covalent bonds or lone pairs, while ELF = 0.5 corresponds to homogeneous electron gases. The 2D ELFs for the lowest enthalpy structures are plotted in Figure 8 (while 2D ELFs for other considered metastable Ti–B structures are plotted in Supporting Information Figure S1). High electron localization can be seen in the region between B atoms, indicating strong covalent B–B bonding. Meanwhile, ELF is negligible at the Ti sites indicating metallic bonding between Ti atoms. Between Ti and B atoms ELF exhibits local maximum values close to the B sites, reflecting partially covalent and partially ionic interactions between Ti and B atoms due to charge transfer from Ti to B. In addition, ELF near the center of the Ti–B bonds is close to 0.5, suggesting a partially metallic bonding feature for the Ti–B bonds. We thus conclude that the chemical bonding in the titanium boride compounds entails a complex combination of covalent, ionic, and metallic characteristics while the strong covalent bonds of B–B and B–Ti are mainly responsible for the high elastic modulus and Vickers hardness (see below).

C. Elastic Properties. As potential near-superhard or superhard materials for engineering applications, the mechanical properties of Ti–B compounds are crucial parameters for assessment. Moreover, the elastic constants can be used to validate the mechanical stability of the materials. The elastic constants are computed using the strain–stress method (see Table 2). As a comparison, experimental results for TiB_2–

DOI: 10.1021/acsami.5b04332
ACS Appl. Mater. Interfaces 2015, 7, 15607–15617

Table 2. Calculated Elastic Constants (GPa), Bulk Modulus (B, GPa), Shear Modulus (G, GPa),Valence Electron Densities (VED, e/Å^3), Young's Modulus (Y, GPa), Poisson's Ratio (ν), and Vickers Hardness (H_v, GPa) of Ti−B Compounds

	c_{11}	c_{22}	c_{33}	c_{12}	c_{13}	c_{23}	c_{44}	c_{55}	c_{66}	B	G	B/G	VED	Y	ν	H_v
TiB−FeB	420	522	420	97	121	65	221	193	175	214	188	1.14	0.329	436	0.160	28.4
TiB−FeB[a]	411	524	410	91	107	61	189	186	193	207	185			427	0.150	
α-TiB	409	434	521	120	95	66	183	182	229	214	189	1.13	0.330	438	0.159	28.5
β-TiB	451		423	100	103		228		183	215	186	1.16	0.330	432	0.165	28.1
TiB_2−AlB_2	652		460	74	115		289		258	261	255	1.02	0.389	578	0.132	38.5 (35[d])
TiB_2−AlB_2[b]	588		503	72	84		238		258	239						
α-TiB_2	554		670	128	95		269		279	**268**	261	1.03	0.391	591	0.132	39.4
β-TiB_2	555		671	125	95		269		281	267	**262**	1.02	0.391	**593**	0.130	**39.6**
Ti_3B_4−Ta_3B_4	582	420	516	106	57	125	241	206	219	232	213	1.09	0.353	488	0.149	32.2
Ti_3B_4−Ta_3B_4[c]	576	423	509	91	55	103	218	227	242	222	219					
α-Ti_3B_4	527	448	514	116	82	112	238	210	218	234	211	1.11	0.354	486	0.154	31.9
β-Ti_3B_4	489		516	116	98		242		218	235	214	1.10	0.354	492	0.152	32.3
Ti_2B−PS_A	278	295	364	96	77	79	76	124	86	160	101	1.58	0.285	249	0.240	15.3
Ti_2B_3−PS_B	432	598	544	109	124	65	244	238	219	240	223	1.08	0.363	511	0.146	33.7
TiB_3−PS_C	649	644	514	72	95	89	270	175	246	257	237	1.08	0.399	544	0.147	35.8
TiB_4−PS_D	648	657	515	73	84	87	261	229	257	255	253	1.01	0.410	571	0.127	38.2

[a]Reference 4. [b]Reference 14. [c]Reference 39. [d]Reference 55.

AlB_2[14] and results from previous theoretical study for TiB−FeB[4] and Ti_3B_4−Ta_3B_4[39] are also listed in Table 2. The bulk modulus and shear modulus can be estimated using the Voigt−Reuss−Hill method,[40−42] and the Young's modulus (Y, GPa) and Possion's ratio (ν) are calculated using the following formulas

$$Y = \frac{9BG}{(3B + G)}$$

$$\nu = \frac{3B - 2G}{2(3B + G)}$$

First, all the Ti−B crystals considered satisfy the mechanical stability criteria,[43] indicating that they are mechanically stable. All positive eigenvalues of the elastic constant matrix further confirm their elastic stability. Taking the orthorhombic crystals as an example, the mechanical stability criteria are given as follows: $C_{11} > 0$, $C_{22} > 0$, $C_{33} > 0$, $C_{44} > 0$, $C_{55} > 0$, $C_{66} > 0$, $[C_{11} + C_{22} + C_{33} + 2(C_{12} + C_{13} + C_{23})] > 0$, $(C_{11} + C_{22} - 2C_{12}) > 0$, $(C_{11} + C_{33} - 2C_{13}) > 0$, and $(C_{22} + C_{33} - 2C_{23}) > 0$. The fact that all Ti−B compounds considered possess relatively high values of C_{11}, C_{22}, and C_{33} implies that these crystals are strong against compression along the a, b, and c axis. Second, the computed shear moduli C_{44} for most compounds (except for Ti_2B−PS_A) are also high, which is another important parameter relevant to the hardness of materials. Among the compounds, TiB_2−AlB_2 has the highest value of C_{44}, thereby a relatively strong shear strength. On the other hand, the values of C_{12}, C_{13}, and C_{23} for these compounds are relatively low, reflecting their weakness in resistance to deformation under biaxial stress conditions (along ab, ac, and bc biaxes). Note that the computed values of elastic constants of TiB_2−AlB_2, TiB−FeB, and Ti_3B_4−Ta_3B_4 are mostly in good agreement with either the measured or previous theoretical values,[4,14,39] confirming reliability of the present calculations.

Materials with high bulk modulus are expected to be strong in resisting uniform compression. As shown in Table 2, the calculated bulk modulus ranges from 160 to 268 GPa, close to that of common hard materials such as Fe_3C (226.8 GPa[44]) and TiC (242 GPa[15]), but less than that of Fe_2B (331 GPa[45]), Cr_7C_3 (300.6 GPa[46]), and WC (400.9 GPa[47]). Among all Ti−B compounds considered, α-TiB_2 possesses the highest bulk modulus (268 GPa). Note also that some previous studies suggest that bulk modulus might have a direct correlation with the valence electron densities (VED).[7,48−50] As for the titanium boride compounds, it appears that the general trend of bulk modulus is consistent with that of VED (except for TiB_3−PS_C and TiB_4−PS_D); i.e., the bulk modulus increases gradually with increasing VED.

It is known that the hardness of materials is more sensitive to the shear modulus than the bulk modulus.[51,52] For the Ti−B compounds considered, their shear modulus (G) and Young's modulus (Y) increase with increasing boron composition initially, and then surge. Like TiB_2−AlB_2, α-TiB_2, β-TiB_2, and TiB_4−PS_D also possess high shear modulus, suggesting that they likely have higher hardness than other Ti−B compounds. In Table 2, it can also be seen that the trend of Poisson's ratio with boron composition is opposite to that of G and Y; i.e., the higher values of G and Y correspond to smaller values of ν. The relatively small Poisson's ratio (<0.2) for almost all Ti−B compounds considered implies their strong covalent bonding. Another important ratio, B/G, represents the materials' ductility. The high (low) B/G ratio means that the material is ductile (brittle), and the critical value is about 1.75.[53] Hence, the relatively low B/G ratio (<1.75) indicates the brittle nature for all Ti−B compounds studied.

A previous study suggests that if a material is intrinsically brittle ($B/G < 1.75$), its hardness can be estimated by Teter's empirical law.[54] Based on this law, we calculate the Vickers hardness of all Ti−B compounds studied (see Table 2). The small difference (3.5 GPa) between the calculated and measured hardness of TiB_2−AlB_2[55] validates this empirical law for the titanium boride compounds. The estimated hardness for all Ti−B compounds studied range from 15.3 to 39.6 GPa. The α-TiB_2 and β-TiB_2 have the highest hardness (39.4 and 39.6 GPa), very close to the lower limit of superhard materials (40 GPa). This high hardness likely stems from the relatively strong B−Ti covalent interaction in both compounds.

CONCLUSION

In conclusion, the lowest energy (or ground state) and low-energy metastable structures of stoichiometric titanium boride

DOI: 10.1021/acsami.5b04332
ACS Appl. Mater. Interfaces 2015, 7, 15607−15617

compounds have been systematically investigated based on the PSO algorithm combined with density functional theory optimization. Besides the three known experimental structures, TiB–FeB, TiB_2–AlB_2, and Ti_3B_4–Ta_3B_4, we predicted two low-energy metastable phases for each of the three compounds, namely, α- and β-Ti_xB_y for TiB, TiB_2, and Ti_3B_4, respectively. Moreover, the lowest energy structures for the four compounds are newly predicted, namely, Ti_2B–PS_A, Ti_2B_3–PS_B, TiB_3–PS_C, and TiB_4–PS_D. In particular, the enthalpy of the predicted Ti_2B–PS_A is lower than that of the previously proposed Ti_2B–Al_2Cu.[32] The obtained convex-hull and phonon spectra confirm that all the newly predicted Ti_2B–PS_A, Ti_2B_3–PS_B, TiB_3–PS_C, and TiB_4–PS_D compounds are thermodynamically stable. Electronic band structure computations show that all Ti–B crystals studied exhibit electronic characteristics of metals, among which the predicted α-TiB_2 and β-TiB_2 exhibit interesting semi-metal-like properties. Further analysis on the computed density of states and electron localization function indicate that strong B–B and Ti–B covalent bonds are present in these Ti–B compounds and the chemical bonding in these compounds is a complex combination of covalent, ionic, and metallic characteristics. Finally, calculations of their mechanical properties reveal that most of the Ti–B compounds studied possess high bulk and shear modulus, as well as low Poisson's ratio and B/G ratio (<1.75). The computed hardness suggests that several of these Ti–B compounds belong to hard materials. In particular, β-TiB_2 has the highest Vickers hardness of 39.6 GPa, very close to the lower limit of superhard materials (40 GPa). We hope that this comprehensive structure search can stimulate future experimental synthesis of the newly predicted near-superhard titanium boride compounds.

■ ASSOCIATED CONTENT

Ⓢ Supporting Information

2D ELFs for metastable Ti–B structures (Figure S1). The Supporting Information is available free of charge on the ACS Publications website at DOI: 10.1021/acsami.5b04332.

■ AUTHOR INFORMATION

Corresponding Authors

*(R.Z.) E-mail: rlzhou@hfut.edu.cn.

*(X.C.Z.) E-mail: xzeng1@unl.edu.

Funding

This work was supported by the USTC Qian-ren B Summer Research Fund and by the University of Nebraska's Holland Computing Center.

Notes

The authors declare no competing financial interest.

■ REFERENCES

(1) Okamoto, N. L.; Kusakari, M.; Tanaka, K.; Inui, H.; Otani, S. Anisotropic Elastic Constants and Thermal Expansivities in Monocrystal CrB_2, TiB_2, and ZrB_2. *Acta Mater.* **2010**, *58*, 76–84.

(2) Kalish, D.; Clougherty, E. V.; Kreder, K. Strength Fracture Mode and Thermal Stress Resistance of HfB_2 and ZrB_2. *J. Am. Ceram. Soc.* **1969**, *52*, 30–36.

(3) Audronis, M.; Kelly, P.; Leyland, A.; Matthews, A. Microstructure of Direct Current and Pulse Magnetron Sputtered Cr–B coatings. *Thin Solid Films* **2006**, *515*, 1511–1516.

(4) Panda, K.; Chandran, K. First Principles Determination of Elastic Constants and Chemical Bonding of Titanium Boride (TiB) on the Basis of Density Functional Theory. *Acta Mater.* **2006**, *54*, 1641–1657.

(5) Xu, J.; Kan, Y.; Liu, W. In-situ Synthetic TiB_2 Particulate Reinforced Metal Matrix Composite Coating on AA2024 Aluminum Alloy by Laser Cladding Technology. *Surf. Rev. Lett.* **2005**, *12*, 561–567.

(6) Scatteia, L.; Alfano, D.; Monteverde, F.; Sans, J. L.; Balat-Pichelin, M. Effect of the Machining Method on the Catalycity and Emissivity of ZrB2 and ZrB2-HfB2-based Ceramics. *J. Am. Ceram. Soc.* **2008**, *91*, 1461–1468.

(7) Chung, H. Y.; Weinberger, M. B.; Levine, J. B.; Kavner, A.; Yang, J. M.; Tolbert, S. H.; Kaner, R. B. Synthesis of Ultra-Incompressible Superhard Rhenium Diboride at Ambient Pressure. *Science* **2007**, *316*, 436–439.

(8) Levine, J. B.; Nguyen, S. L.; Rasool, H. I.; Wright, J. A.; Brown, S. E.; Kaner, R. B. Preparation and Properties of Metallic, Superhard Rhenium Diboride Crystals. *J. Am. Chem. Soc.* **2008**, *130*, 16953–16958.

(9) Gu, Q. F.; Krauss, G.; Steurer, W. Transition Metal Borides: Superhard versus Ultra-incompressible. *Adv. Mater.* **2008**, *20*, 3620–3626.

(10) Wang, B.; Li, X.; Wang, Y. X.; Tu, Y. F. Phase Stability and Physical Properties of Manganese Borides: A First-Principles Study. *J. Phys. Chem. C* **2011**, *115*, 21429–21435.

(11) Decker, B. F.; Kasper, J. S. The Crystal Structure of TiB. *Acta Crystallogr.* **1954**, *7*, 77–81.

(12) Murray, J. L.; Liao, P. K.; Spear, K. E. The B–Ti (Boron-Titanium) System. *Bull. Alloy Phase Diagrams* **1986**, *7*, 550–555.

(13) Spear, K. E.; Mcdowell, P.; Mcmahon, F. Experimental-evidence for the Existence of the Ti_3B_4 Phase. *J. Am. Ceram. Soc.* **1986**, *69*, C-4–C-5.

(14) Manghnani, M. H.; Fisher, E. S.; Li, F. Y.; Grady, D. E. Elastic Moduli of TiB_2. *Ceram. Trans.* **1993**, *38*, 771–785.

(15) Gilman, J. J.; Roberts, B. W. Elastic Constants of TiC and TiB_2. *J. Appl. Phys.* **1961**, *32*, 1405.

(16) Milman, V.; Warren, M. C. Elastic Properties of TiB2 and MgB2. *J. Phys.: Condens. Matter* **2001**, *13*, 5585–5595.

(17) Perottoni, C. A.; Pereira, A. S.; Jornada, J. A. H. d. Periodic Hartree-Fock Linear Combination of Crystalline Orbitals Calculation of the Structure, Equation of State and Elastic Properties of Titanium Diboride. *J. Phys.: Condens. Matter* **2000**, *12*, 7205–7222.

(18) Peng, F.; Fu, H. Z.; Cheng, X. L. First-principles Calculations of Thermodynamic Properties of TiB2 at High Pressure. *Phys. B* **2007**, *400*, 83–87.

(19) Spoor, P. S.; Maynard, J. D.; Pan, J. M.; Green, D. J.; Hellmann, J. R.; Tanaka, T. Elastic Constants and Crystal Anisotropy of Titanium Diboride. *Appl. Phys. Lett.* **1997**, *70*, 1959–1961.

(20) Feng, H. B.; Zhou, Y.; Jia, D. C.; Meng, Q. C.; Rao, J. C. *Cryst. Growth Des.* **2006**, *6*, 1626–1630.

(21) Ma, X.; Li, C.; Du, Z.; Zhang, W. Thermodynamic Assessment of the Ti-B System. *J. Alloys Compd.* **2004**, *370*, 149–158.

(22) Wang, Y.; Lv, J.; Zhu, L.; Ma, Y. Crystal Structure Prediction via Particle-swarm Optimization. *Phys. Rev. B: Condens. Matter Mater. Phys.* **2010**, *82*, 094116(1–8).

(23) Ma, Y.; Eremets, M. I.; Oganov, A. R.; Xie, Y.; Trojan, I.; Medvedev, S.; Lyakhov, A. O.; Valle, M.; Prakapenka, V. Transparent Dense Sodium. *Nature* **2009**, *458*, 182–185.

(24) Oganov, A. R.; Ma, Y. M.; Xu, Y.; Errea, I.; Bergara, A.; Lyakhov, A. O. Exotic Behavior and Crystal Structures of Calcium under Pressure. *Proc. Natl. Acad. Sci. U. S. A.* **2010**, *107*, 7646–7651.

(25) Xie, Y.; Oganov, A. R.; Ma, Y. Novel High Pressure Structures and Superconductivity of CaLi2. *Phys. Rev. Lett.* **2010**, *104*, 177005(1–4).

(26) (a) Zhou, R. L.; Zeng, X. C. Polymorphic Phases of Sp3-Hybridized Carbon under Cold Compression. *J. Am. Chem. Soc.* **2012**, *134*, 7530–7538. (b) Zhou, R.; Qu, B.; Dai, J.; Zeng, X. C. Unraveling Crystalline Structure of High-Pressure Phase of Silicon Carbonate. *Phys. Rev. X* **2014**, *4*, 011030(1–11).

(27) (a) Peng, F.; Miao, M. S.; Wang, H.; Li, Q.; Ma, Y. M. Predicted Lithium–Boron Compounds under High Pressure. *J. Am. Chem. Soc.* **2012**, *134*, 18599–18605. (b) Zhao, Z. S.; Tian, F.; Dong, X.; Li, Q.;

DOI: 10.1021/acsami.5b04332
ACS Appl. Mater. Interfaces 2015, 7, 15607–15617

Wang, Q. Q.; Wang, H.; Zhong, X.; Xu, B.; Yu, D. L.; He, J. L.; Wang, H. T.; Ma, Y. M.; Tian, Y. J. Tetragonal Allotrope of Group 14 Elements. *J. Am. Chem. Soc.* **2012**, *134*, 12362−12365. (c) Li, P. F.; Zhou, R. L.; Zeng, X. C. The search for the most stable structures of silicon carbon monolayer compounds. *Nanoscale* **2014**, *6*, 11685−11691. (d) Dai, J.; Wu, X. J.; Yang, J. L.; Zeng, X. C. Al_xC Monolayer Sheets: Two-Dimensional Networks with Planar Tetracoordinate Carbon and Potential Applications as Donor Materials in Solar Cell. *J. Phys. Chem. Lett* **2014**, *5*, 2058−2065. (e) Dai, J.; Zhao, Y.; Wu, X. J.; Yang, J. L.; Zeng, X. C. Exploration of Structures of Two-Dimensional Boron−Silicon Compounds with sp^2 Silicon. *J. Phys. Chem. Lett* **2013**, *4*, 561−567.

(28) Dai, J.; Wu, X. J.; Yang, J. L.; Zeng, X. C. Unusual Metallic Microporous Boron Nitride Networks. *J. Phys. Chem. Lett.* **2013**, *4*, 3484−3488.

(29) Perdew, J. P.; Burke, K.; Ernzerhof, M. Generalized Gradient Approximation Made Simple. *Phys. Rev. Lett.* **1996**, *77*, 3865−3868.

(30) Kresse, G.; Furthmüller, J. Efficient Iterative Schemes for ab initio Total-energy Calculations Using a Plane-wave Basis Set. *Phys. Rev. B: Condens. Matter Mater. Phys.* **1996**, *54*, 11169−11186.

(31) Togo, A.; Oba, F.; Tanaka, I. First-principles Calculations of the Ferroelastic Transition between Rutile-type and CaCl2-type SiO2 at High Pressures. *Phys. Rev. B: Condens. Matter Mater. Phys.* **2008**, *78*, 134106(1−9).

(32) Mohn, P. The Calculated Electronic and Magnetic Properties of the Tetragonal Transition-metal Semi-borides. *J. Phys. C: Solid State Phys.* **1988**, *21*, 2841−2851.

(33) Rühl, R.; Jeitschko, W. Preparation and Structure of Technetium Triphosphide and Rhenium Triphosphide, Isotypic Polyphosphides with Metal Chains. *Acta Crystallogr., Sect. B: Struct. Crystallogr. Cryst. Chem.* **1982**, *38*, 2784−2788.

(34) Fu, Y.-Y.; Li, Y.-W.; Huang, H.-M. Elastic and Dynamical Properties of YB_4: First-Principles Study. *Chin. Phys. Lett.* **2014**, *31*, 116201(1−4).

(35) Ghosh, G.; van de Walle, A.; Asta, M. First-Principles Calculations of the Structural and Thermodynamic Properties of bcc, fcc and hcp Solid Solutions in the Al−TM (TM = Ti, Zr and Hf) Systems: A Comparison of Cluster Expansion and Supercell Methods. *Acta Mater.* **2008**, *56*, 3202−3221.

(36) Zhang, X. W.; Trimarchi, G.; Zunger, A. Possible Pitfalls in Theoretical Determination of Ground-State Crystal Structures: The Case of Platinum Nitride. *Phys. Rev. B: Condens. Matter Mater. Phys.* **2009**, *79*, 092102(1−4).

(37) Ashcroft, N. W.; Mermin, N. D. *Solid State Physics*; Holt, Rinehart and Winston: New York, 1976.

(38) Vajeeston, P.; Ravindran, P.; Ravi, C.; Asokamani, R. Electronic Structure, Bonding, and Ground-State Properties of AlB_2-type Transition-Metal Diborides. *Phys. Rev. B: Condens. Matter Mater. Phys.* **2001**, *63*, 045115(1−12).

(39) Sun, L.; Gao, Y.; Xiao, B.; Li, Y.; Wang, G. Anisotropic Elastic and Thermal Properties of Titanium Borides by First-principles Calculations. *J. Alloys Compd.* **2013**, *579*, 457−467.

(40) Voigt. W. *Lehrburch der Kristallphysik*; Teubner: Leipzig, Germany, 1928.

(41) Reuss, A. Z. Berechnung der Fließgrenze von Mischkristallen auf Grund der Plastizitätsbedingung für Einkristalle. *Z. Angew. Math. Mech.* **1929**, *9*, 49−58.

(42) Hill, R. The Elastic Behaviour of a Crystalline Aggregate. *Proc. Phys. Soc., London, Sect. A* **1952**, *65*, 349−354.

(43) Wu, Z.-j.; Zhao, E.-j.; Xiang, H.-p.; Hao, X.-f.; Liu, X.-j.; Meng, J. Crystal Structures and Elastic Properties of Superhard IrN2 and IrN3 from First Principles. *Phys. Rev. B: Condens. Matter Mater. Phys.* **2007**, *76*, 054115(1−15).

(44) Jang, J. H.; Kim, I. G.; Bhadeshia, H. K. D. H. Substitutional Solution of Silicon in Cementite: A First-principles Study. *Comput. Mater. Sci.* **2009**, *44*, 1319−1326.

(45) Price, D. L.; Cooper, B. R. Total Energies and Bonding for Crystallographic Structures in Titanium-carbon and Tungsten-carbon Systems. *Phys. Rev. B: Condens. Matter Mater. Phys.* **1989**, *39*, 4945−4957.

(46) Li, Y.; Gao, Y.; Xiao, B.; Min, T.; Yang, Y.; Ma, S.; Yi, D. The Electronic, Mechanical Properties and Theoretical Hardness of Chromium Carbides by First-Principles Calculations. *J. Alloys Compd.* **2011**, *509*, 5242−5249.

(47) Li, Y. F.; Gao, Y. M.; Xiao, B.; Min, T.; Fan, Z. J.; Ma, S. Q.; Xu, L. L. Theoretical Study on the Stability, Elasticity, Hardness and Electronic Structures of W−C Binary Compounds. *J. Alloys Compd.* **2010**, *502*, 28−37.

(48) Kaner, R. B.; Gilman, J. J.; Tolbert, S. H. Designing Superhard Materials. *Science* **2005**, *308*, 1268−1269.

(49) Li, C. H.; Wu, P. Correlation of Bulk Modulus and the Constituent Element Properties of Binary Intermetallic Compounds. *Chem. Mater.* **2001**, *13*, 4642−4648.

(50) Cumberland, R. W.; Weinberger, M. B.; Gilman, J. J.; Clark, S. M.; Tolbert, S. H.; Kaner, R. B. Osmium Diboride, An Ultra-Incompressible, Hard Material. *J. Am. Chem. Soc.* **2005**, *127*, 7264−7265.

(51) Guo, W. L.; Liang, Y. C.; Fang, Z. First Principles Studies of Low-compressibility of Transition-metal Compounds OsB_2 and OsO_2. *Acta Phys. Sin.* **2007**, *56*, 4847−4855.

(52) Fulcher, B. D.; Cui, X. Y.; Delley, B.; Stampfl, C. Hardness Analysis of Cubic Metal Mononitrides from First Principles. *Phys. Rev. B: Condens. Matter Mater. Phys.* **2012**, *85*, 184106(1−9).

(53) Pugh, S. F. Relations between the Elastic Moduli and the Plastic Properties of Polycrystalline Pure Metals. *Philos. Mag.* **1954**, *45*, 823−843.

(54) Teter, D. M. Computational Alchemy: The Search for New Superhard Materials. *MRS Bull.* **1998**, *23*, 22−27.

(55) Zhang, X.; Luo, X.; Li, J.; Hu, P.; Han, J. The Ideal Strength of Transition Metal Diborides TMB_2 (TM = Ti, Zr, Hf): Plastic Anisotropy and the role of Prismatic Slip. *Scr. Mater.* **2010**, *62*, 625−628.

DOI: 10.1021/acsami.5b04332
ACS Appl. Mater. Interfaces 2015, 7, 15607−15617